Shell-Thickness Controlled Semiconductor–Metal Transition in Si–SiC Core–Shell Nanowires

ARTICLE *in* NANO LETTERS · APRIL 2015

Impact Factor: 13.59 · DOI: 10.1021/acs.nanolett.5b00670 · Source: PubMed

2 AUTHORS:

Michele Amato
Université Paris-Sud 11
21 PUBLICATIONS **265** CITATIONS
SEE PROFILE

Riccardo Rurali
Materials Science Institute of Barcelona
113 PUBLICATIONS **2,194** CITATIONS
SEE PROFILE

NANO LETTERS

Letter

pubs.acs.org/NanoLett

Shell-Thickness Controlled Semiconductor–Metal Transition in Si–SiC Core–Shell Nanowires

Michele Amato[†] and Riccardo Rurali*[,‡]

[†]Institut d'Electronique Fondamentale, UMR8622, CNRS, Université Paris Sud, 91405 Orsay, France

[‡]Institut de Ciència de Materials de Barcelona (ICMAB-CSIC), Campus de Bellaterra, 08193 Bellaterra, Barcelona, Spain

Supporting Information

ABSTRACT: We study Si–SiC core–shell nanowires by means of electronic structure first-principles calculations. We show that the strain induced by the growth of a lattice-mismatched SiC shell can drive a semiconductor–metal transition, which in the case of ultrathin Si cores is already observed for shells of more than one monolayer. Core–shell nanowires with thicker cores, however, remain semiconducting even when four SiC monolayers are grown, paving the way to versatile, biocompatible nanowire-based sensors.

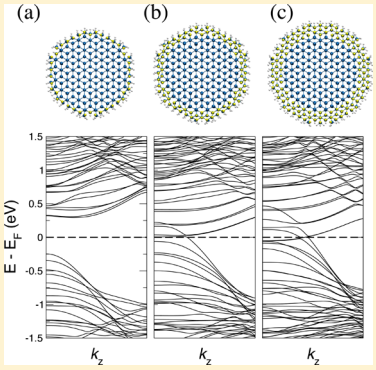

KEYWORDS: *Si–SiC, core–shell, first-principles calculations, nanowires, strain*

Among the many applications that have been demonstrated for semiconducting nanowires,[1,2] chemical sensing is certainly one of the most promising.[3−5] The large surface-to-volume ratio and the possibility to tune their properties at growth time, controlling the composition, crystal orientation, and diameter, make nanowires bound to outperform any other conventional alternative in a large class of sensing environments. The tremendous development of nanomedicine has catalyzed much of the research in nanosensors, and nanowires are no exception:[6,7] ultrasensitive detection of DNA,[8,9] as well as sensing of proteins[10,11] and viruses[12] have been successfully demonstrated.

When it comes to sensors for biological environments, an important feature is biocompatibility, which broadly speaking refers to the way materials interact with the human body.[13] Biocompatibility is an elusive notion, though, because it normally depends on how and where the material is used. Yet, there is a general consensus on the fact that the chemically inert and hydrophilic surface of SiC makes it a much better biocompatible material than Si.[14−18]

In this regard, the cubic polytype, 3C-SiC, is a particularly appealing biomaterial, because of its high surface wettability and biocompatibility if compared with Si.[19] The SiC noticeable capability to be functionalized with biomolecules and biological systems has been demonstrated in many medical applications like the construction of myocardial biosensors,[20] the coating of neural probes,[21] and the hard coatings for coronary heart stents.[22,23] Moreover, its ease to be grown on Si substrates[24−29] and its extraordinary electronic properties, i.e., wide band gap, large electron mobility, high saturation drift velocity, and high dielectric breakdown field,[30] are clear signs of its remarkable potential as active component of electronic devices. Therefore, one can envisage a biosensor whose backbone is made of Si, thus easily embedded into the existing technology, and where the interface between the electronic and biological world is mediated by the more biocompatible 3C-SiC surface.[18,19] A major challenge for this architecture is the huge lattice mismatch between Si and 3C-SiC both in lattice parameters (19% at room temperature) and in thermal expansion coefficients (23% at deposition temperatures and 8% at room temperatures).[31] As a matter of fact, planar and volume defects, high residual stress and voids deriving by this mismatch can be reduced only by carefully modulating temperature and pressure conditions during the heteroepitaxial growth.[31] Indeed, the possibility of increasing the interface quality in 3C-SiC–Si epitaxial layers has been demonstrated in many different experimental works.[31−35] These ideas can be in principle transferred to the nanowire geometry, and in fact, single crystalline Si core SiC shell NWs with abrupt, well-defined interfaces have been reported recently.[36] However, despite a few experimental reports on the growth of Si–SiC core–shell nanostructures,[36−42] little is known about their electronic properties.

In this Letter we intend to fill this gap, investigating with first-principles atomistic calculations different core–shell structures and assessing their viability as efficient biosensors.

Received: February 25, 2015
Revised: March 25, 2015

DOI: 10.1021/acs.nanolett.5b00670
Nano Lett. XXXX, XXX, XXX–XXX

Our calculations highlight two major points: (i) first, for ultrathin Si−SiC core−shell NWs the presence of a thicker shell (more than one monolayer) has a drastic effect on the electronic structure leading to a semiconductor-metal transition; (ii) this occurrence is fortunately not observed in the case of larger diameter wires, which remain semiconducting also for four monolayer (ML) shells assessing their potential as biocompatible nanostructures.

We perform density functional theory (DFT) calculations within the generalized gradient approximation (GGA)[43] with the SIESTA code.[44] Thicker core−shell nanowires, with up to ∼10 000 atoms, have been studied with a bond-order, classical potential due to Tersoff.[45] A detailed description of the calculations can be found in the Supporting Information.

We have studied nanowires grown along the ⟨111⟩ orientation, where a 2.5 nm Si core is wrapped by a 1-, 2-, 3-, and 4-monolayer (ML) 3C-SiC shell. Experimental evidence of defect-free epitaxial Si−SiC core−shell with 1−2 ML shells has been recently reported.[36,46] Yet, we have also considered the case of a shell made up by 3 and 4 ML because of the many demonstrations that the cylindrical geometry of nanowires can allow for additional stress release, leading to clean epitaxies that are forbidden in two-dimensional interfaces, e.g., defect-free Si−Ge axial interfaces,[47,48] conformal Si shells of up to 3 nm around a Ge core of 32 nm (three times larger than the critical thickness for planar Si/Ge heteroepitaxial growth).[49] However, a note of caution is in order here because a detailed understanding of basic phenomena in 3C-SiC/Si cylindrical interfaces at the nanoscale is still lacking, and more experimental work has to be conducted in this direction.

The band-structures of three cases of Si−SiC core−shell NWs (with 1, 2, and 3 ML shell), together with a cross-section view, are displayed in Figure 1. As can be seen, when more the one SiC ML is grown around the Si core the wire becomes metallic (results for 4 ML shell are not discussed, but the physical behavior is very similar to the case of 3 ML). It is unlikely that a type-III, broken-gap band offset develops at the Si−SiC interface because of the much larger band gap of SiC with respect to Si.[50] However, to give a closer look at the electronic structure around the Fermi level we have studied the projected density of states (pDOS) on the basis functions centered around atoms of the Si core and of the SiC shell (see Figure 2, left panel). The analysis of the band-offset is rather straightforward in the case of the 1 ML SiC shell, which is semiconducting (see Figure 2, top row). It is clear that both the top of the valence band and the bottom of the conduction band are localized on the Si core, and while having such thin shells is difficult to make a quantitative estimate, the band-offset is type-I. This is supported by the spatial distribution of the wave function of the band-edge states plotted on the right-hand side of Figure 2. This picture does not qualitatively change when more SiC MLs are added (see Figure 2, bottom row): the states at the Fermi level are largely dominated by core states, although sometimes they mix with shell states (see, for instance, the second state selected for the 3 ML shell). Therefore, the band gap is *closed* by Si core states and not by a type-III-like overlap of core (Si) and shell (SiC) states.

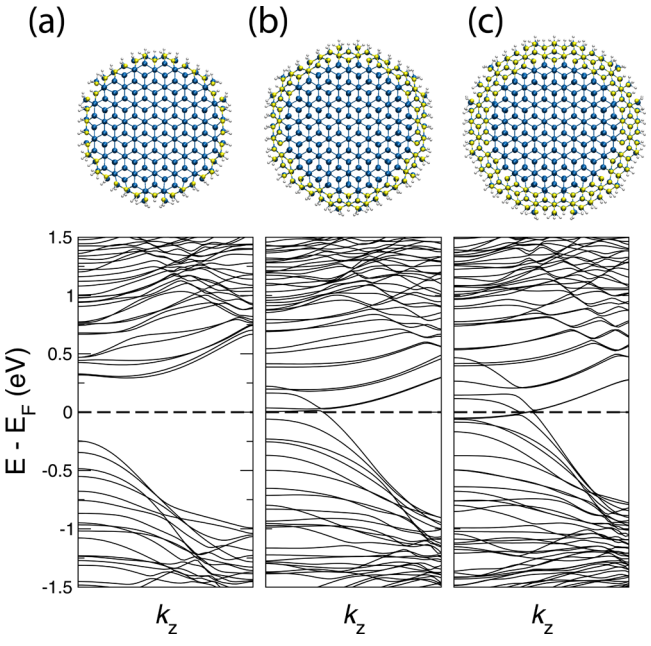

Figure 1. Cross-section view and band-structure diagram of a Si core SiC shell NW with a core of 2.5 nm and a shell of (a) 1, (b) 2, and (c) 3 MLs of SiC. Blue, yellow, and white spheres represent Si, C, and H atoms, respectively.

This analysis leads to the conclusion that the metallicity of the Si core likely arises because of the compressive strain induced by the lattice-mismatched SiC shell. In order to prove that, we have compared the band-structures of a stand-alone Si NW of the same diameter of the core of the wires of Figure 1 with the degree of strain imposed by the SiC shell, i.e., the equilibrium lattice parameter of the core−shell NWs, summarized in Table 1. The results show that, indeed, increasing the strain at first shrinks the Si NW band gap, until it closes it completely, with the valence and conduction band of the unstrained NW (marked with two circles in 3) crossing. The same eigenstates are easily recognizable in the band-structure of the core−shell NWs (Figure 1). The values of the applied strain in Figure 3, 3.9%, 8.7%, and 10.1%, have been chosen by fixing the axial lattice parameter a_z to the optimized values of the core−shell NW with 1, 2, and 3 ML SiC shells. This effect is general and can be reproduced, for instance, in nanowires grown along the ⟨110⟩ orientation (see the Supporting Information).

The strain-driven band gap engineering of a nanowire through the growth of a lattice mismatched shell is certainly intriguing, particularly if it can lead to a semiconductor−metal transition, but sensing applications require the material to be robustly semiconducting. Our results indicate that 1 ML SiC shell around a thin Si core, while providing the Si-based device with a biocompatible sheath, would comply with this requirement. Fortunately, this is within current experimental capabilities, as abrupt, defect-free Si−SiC interfaces, with 1 ML SiC shells, have been reported.[36] Increasing the thickness of the shell would lead to the formation of interface defects such as dislocations, and voids, though, of 2 and, perhaps, 3 ML high crystalline shells could still be grown epitaxially in nanowire geometry. As discussed above, this situation should be avoided, at least for ultrathin Si cores, because the core−shell NW would turn into a one-dimensional metal. At the same time, extended coordination defects could help releasing the interfacial strain, though their effect on the electronic structure of the core−shell system should be carefully analyzed.

The growth of a 1 ML SiC shell reduces the band gap to approximately one-half of the value of the unstrained Si NWs. However, the rest of the parameters that are relevant to the

DOI: 10.1021/acs.nanolett.5b00670
Nano Lett. XXXX, XXX, XXX−XXX

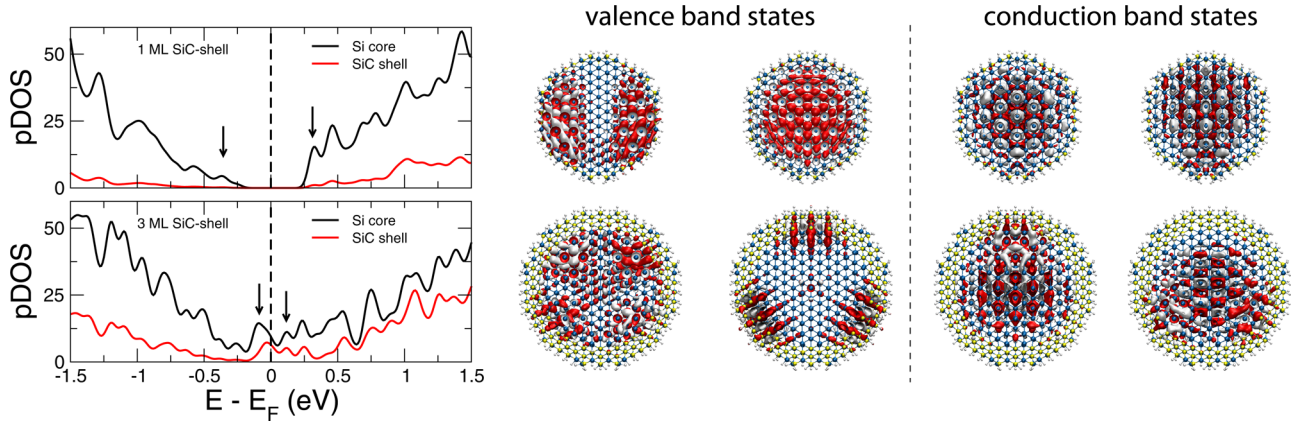

Figure 2. (left) Projections of the total DOS on the basis functions centered around atoms of the Si core and of the SiC shell for 1 ML SiC shell (top row) and 3 ML SiC shell (bottom row). (right) Wave functions at the Γ point of four eigenstates around the Fermi level. The energy of these states is indicated by small arrows in the pDOS plots on the left-hand side.

Table 1. Equilibrium Lattice Parameter and Equivalent Applied Strain on the Si Core for the Core−Shell NWs Considered

#ML SiC shell	a_z (Å)	strain (%)
	9.330	0.0
1	8.968	3.9
2	8.519	8.7
3	8.391	10.1

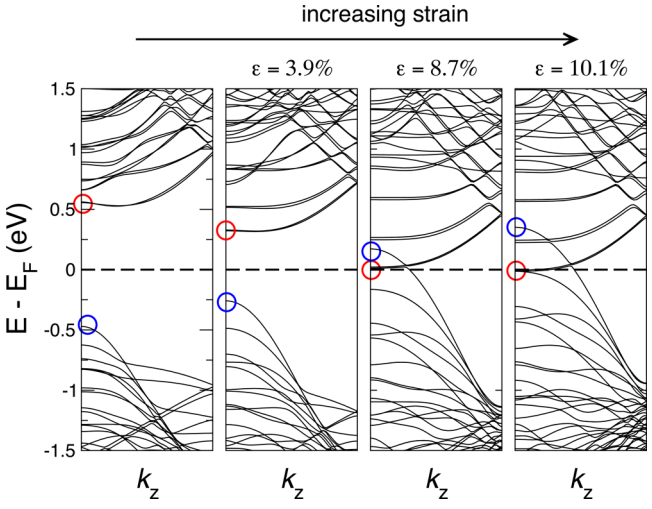

Figure 3. Band-structure diagrams of a Si NW of the same diameter of the Si core of the core−shell NWs of Figure 1 at different degrees of strain, ϵ. (left) Unstrained ground state; (mid left) ϵ = 3.9%, corresponding to the strain induced by a 1 ML SiC shell; (mid right) ϵ = 8.7%, corresponding to the strain induced by a 2 ML SiC shell; and (right) ϵ = 10.1%, corresponding to the strain induced by a 3 ML SiC shell. The red and blue circles help to track the evolution of the unstrained wire band-edges as the strain increases.

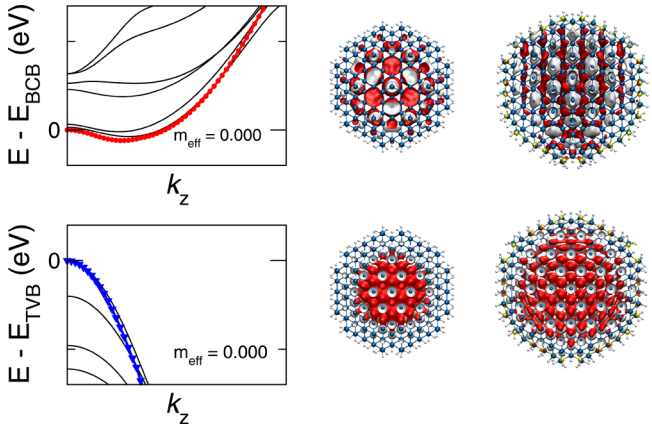

Figure 4. (left) Top of the valence band and bottom of the conduction band eigenstates of the 2.5 nm Si NW are shown over the band-structure diagram of the core−shell NW with a 1 ML SiC shell. The bands of the Si NW in red and blue have been suitably shifted to account for the narrowing of the energy gap of the core−shell NW. (right) Wave function at the Γ point of the unstrained Si NW and the semiconducting Si−SiC core−shell NW. The valence band retains its symmetry, while hybridization with shell states results in a non-negligible distortion of the conduction band wave function (the conduction band is triple degenerate; here, we plot only one state for the sake of the argument).

metrics of a nanosensor, such as the effective masses, the slightly indirect character of the band gap (the fundamental gap is ∼25−30 meV narrower than the direct gap at Γ), and the symmetry of the wave functions, are largely unaffected, as shown in Figure 4. It is also worth noting that, although for the sake of simplicity we have terminated the surface dangling bonds with hydrogen atoms, in experimentally grown nanowires the outer SiC shell would be covered with a native SiO_2 sheath. The oxidation of the surface can strongly affect the chemical response of the SiC shell and hence its potential use in biosensing. This subject has been quite intensively studied. Interestingly, it has been shown that (i) the formation of a native oxide on the SiC surface facilitates its chemical functionalization, a prerequisite in the realization of sensing devices, and that (ii) the SiO_2/SiC interface is more easily chemically modified than SiO_2/Si system (which is instead an unsuitable material for biochemical field effect devices).[19,51]

The compressive strain induced by a SiC shell on a Si core should roughly depend on the ratio between the core and shell thickness. However, this linear dependence, known as Vegard's law,[52,53] works well with materials with not too different of lattice constants,[54−56] but does not necessarily hold for strongly lattice-mismatched materials such as Si and SiC. Hence, we decided to test it by considering 1−4 SiC MLs around a Si core with diameter ranging from 6 to 14 nm. These structures, which contain from 902 to 9614 atoms, cannot be handled

DOI: 10.1021/acs.nanolett.5b00670
Nano Lett. XXXX, XXX, XXX−XXX

efficiently at the DFT level; thus, we optimized the atomic positions and the axial lattice parameter with a classical potential for Si−C systems due to Tersoff.[45] We tested it against DFT in a 2.5 nm diameter structure similar to the one of Figure 1a, obtaining values of the lattice parameter within 0.45%. The strain, calculated as $(a_z^{Si-SiC} - a_z^{Si})/a_z^{Si}$, as a function of the number of SiC MLs is plotted in Figure 5. The values of

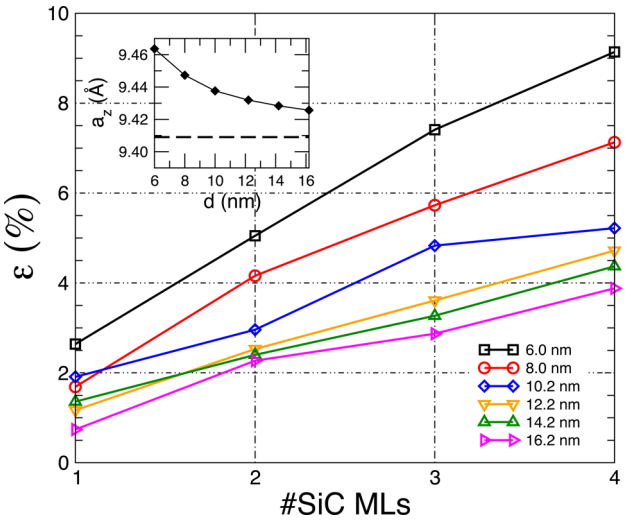

Figure 5. Compressive strain of the Si core as a function of the SiC shell thickness for different core diameters. The inset shows the unstrained value (without SiC shell) of the axial lattice parameter of Si NW as a function of the diameter; the dashed line indicates the bulk limit.

a_z^{Si} depend on the diameter and are shown in the inset. The strain increases roughly linearly, in agreement with the predictions of Vegard's law, and the thicker the Si core, the lower the strain induced by the SiC shell. As can be seen, in the case of the growth of 1−2 MLs the resulting strain on the Si core is at most 5%, a value that goes down to ∼2% if cores of more than 10 nm are considered.

In order to predict if any of these wires can undergo the strain-induced metallization that we have reported above for an ultrathin 2.5 nm NW, we have mapped the evolution of bulk Si band-structure to make an estimate (Figure 6). The conduction band minimum (CBM) along the Γ−X direction, X'_{CBM}, decreases, while the valence band maximum at Γ, Γ_{VBM}, simultaneously increases. As a result of these behaviors (Figure 6, top), the gap, which is initially indirect at Γ−X′, closes for a compressive strain of ∼9%, a value approached only in the most critical case considered (6 nm core plus a 4 SiC ML shell, black diamond in Figure 5). Notice that while DFT is known to describe with great accuracy the pressure coefficients of the bands of Si-based systems,[57,58] the band gap is notoriously underestimated. This means that the lines in Figure 6 (bottom panel) would cross at even larger strains than those indicated, being 9%, a quite conservative lower bound. The same observation applies to the case of nanowires. These results indicate that Si−SiC core−shell NWs with a thicker than 10 nm core and a realistic 1−4 ML shell are safely semiconducting and have a type-I band-offset, with both band-edge states localized on the Si core. This conclusion is consistent with the rectifying behavior of Si−SiC core−shell NW-based nano-FET recently observed by Ollivier et al.:[59] even if they considered larger structures than those of the present study, their findings

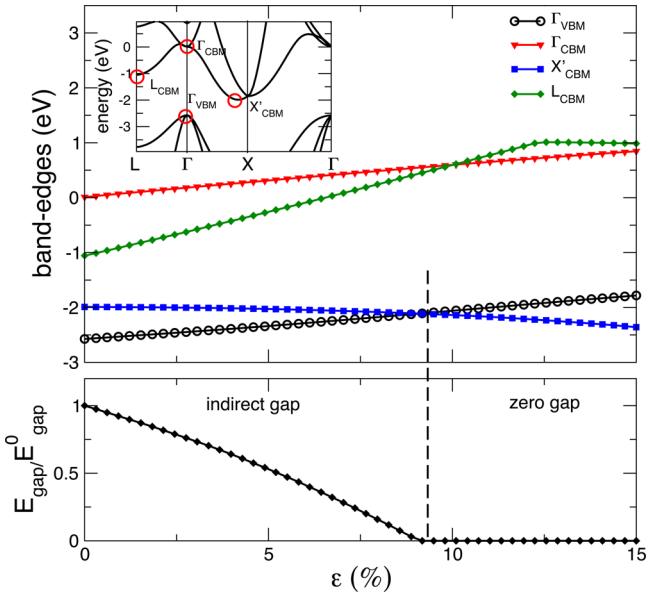

Figure 6. (top) Dependence on the compressive hydrostatic strain of a few relevant eigenvalues of bulk Si bands. The tracked eigenvalues are identified with circles in the ground-state unstrained band-structure in the inset. (bottom) Band-gap as a function of the applied hydrostatic strain. The gap, initially indirect at Γ−X′, closes as a result of a combined increase and decrease of the Γ_{VBM} and X'_{CBM}, respectively. The change of slope of L_{CBM} is due to a band crossing at the L point at large strains. The gap closes at larger strain values if its underestimation within DFT is taken into account.

represent a robust experimental evidence that Si−SiC core−shell NWs remain semiconducting for large core/shell ratios.

In summary, we have explored by density functional calculations the rich physics of Si−SiC core−shell NWs. We have shown that a SiC shell that is thick enough in comparison with the Si core can drive a semiconductor−metal transition because of the large compressive strain. A system that stays semiconducting, however, offers a very interesting perspective for its use as sensor in biological environments: the Si core maintains its transport properties, with a mobility that is roughly insensitive to the presence of the shell, but benefits from the protection of the biocompatible SiC shell. We expect that a variation of the shell thickness beyond the size here analyzed will only marginally affect the type I band offset in the wire, though it can alter its transport properties upon biomolecule absorption.[60] The semiconductor−metal transition described only interests very thin wires that, although within the current experimental capabilities,[61−66] are not routinely grown. Thick enough SiC shells could result in a similar effect also in thicker wires, but interface defects are then expected to develop, releasing the interface strain. Calculations based on classical potentials indicate that in all the cases of practical interest, as confirmed by recent experiments,[59] a Si−SiC core−shell NW is semiconducting. The role of misfit dislocations, expected for shells thicker than 1−3 MLs, and the physics of dopants (activation energy, interface segregation) in these highly strained structures is yet to be clarified.

■ ASSOCIATED CONTENT

Supporting Information

Computational details; ⟨110⟩ nanowires; band-structure diagrams of a ⟨110⟩ Si NW of the same diameter of the Si

DOI: 10.1021/acs.nanolett.5b00670
Nano Lett. XXXX, XXX, XXX−XXX

core of the core−shell NWs in Figure 1. This material is available free of charge via the Internet at http://pubs.acs.org.

AUTHOR INFORMATION

Corresponding Author

*E-mail: rrurali@icmab.es.

Notes

The authors declare no competing financial interest.

ACKNOWLEDGMENTS

We acknowledge support under contract no. FEDER-FIS2012-37549-C05-05 of the Ministerio de Economía y Competitividad (MINECO) and grant 2014 SGR 301 of the Generalitat de Catalunya. We thank the Centro de Supercomputación de Galicia (CESGA) for the use of their computational resource. M.A. thankfully acknowledges the computer resources, technical expertise, and assistance provided by the Red Española de Supercomputación. Support from Psi-k/ESF is greatly acknowledged.

REFERENCES

(1) Lu, W.; Lieber, C. M. *J. Phys. D: Appl. Phys.* **2006**, *39*, R387−R406.
(2) Rurali, R. *Rev. Mod. Phys.* **2010**, *82*, 427−449.
(3) Cui, Y.; Wei, Q.; Park, H.; Lieber, C. M. *Science* **2001**, *293*, 1289−1292.
(4) Zhou, X. T.; Hu, J. Q.; Li, C. P.; Ma, D. D. D.; Lee, C. S.; Lee, S. T. *Chem. Phys. Lett.* **2003**, *369*, 220−224.
(5) Patolsky, F.; Lieber, C. M. *Mater. Today* **2005**, *8*, 20−28.
(6) Stern, E.; Klemic, J. F.; Routenberg, D. A.; Wyrembak, P. N.; Turner-Evans, D. B.; Hamilton, A. D.; LaVan, A. D.; Fahmy, T. M.; Reed, M. A. *Nature* **2006**, *445*, 519−522.
(7) Patolsky, F.; Zheng, G.; Lieber, C. M. *Nanomedicine* **2006**, *1*, 51−65.
(8) Hahm, J.-i.; Lieber, C. M. *Nano Lett.* **2004**, *4*, 51−54.
(9) Li, Z.; Chen, Y.; Li, X.; Kamins, T.; Nauka, K.; Williams, R. *Nano Lett.* **2004**, *4*, 245−247.
(10) Tang, T.; Liu, X.; Li, C.; Lei, B.; Zhang, D.; Rouhanizadeh, M.; Hsiai, T.; Zhou, C. *Appl. Phys. Lett.* **2005**, *86*, 103903.
(11) Zheng, G.; Patolsky, F.; Cui, Y.; Wang, W. U.; Lieber, C. M. *Nat. Biotechnol.* **2005**, *23*, 1294−1301.
(12) Patolsky, F.; Zheng, G.; Hayden, O.; Lakadamyali, M.; Zhuang, X.; Lieber, C. M. *Proc. Natl. Acad. Sci. U.S.A.* **2004**, *101*, 14017−14022.
(13) Williams, D. F. *Biomaterials* **2008**, *29*, 2941−2953.
(14) Yakimova, R.; Petoral, R. M., Jr.; Yazdi, G. R.; Vahlberg, C.; Spetz, A. L.; Uvdal, K. *J. Phys. D: Appl. Phys.* **2007**, *40*, 6435.
(15) Cogan, S. F.; Edell, D. J.; Guzelian, A. A.; Ping Liu, Y.; Edell, R. *J. Biomed. Mater. Res.* **2003**, *67A*, 856.
(16) Chapman, T. *Nature* **2005**, *434*, 795.
(17) Saddow, S. E.; Frewin, C. L.; Coletti, C.; Schettini, N.; Weeber, E.; Oliveros, A.; Jarosezski, M. *Mater. Sci. Forum* **2011**, *679−680*, 824−830.
(18) Mahmoodi, M.; Ghazanfari, L. In *Physics and Technology of Silicon Carbide Devices*; Hijikata, Y., Ed.; InTech: Rijeka, Croatia, 2012; Chapter 15, pp 349−378.
(19) Oliveros, A.; Guiseppi-Elie, A.; Saddow, S. *Biomed. Microdevices* **2013**, *15*, 353−368.
(20) Godignon, P. *Mater. Sci. Forum* **2005**, *483−485*, 1009−1014.
(21) Hsu, J.-M.; Tathireddy, P.; Rieth, L.; Normann, A. R.; Solzbacher, F. *Thin Solid Films* **2007**, *516*, 34−41.
(22) Rzany, A.; Harder, C.; Schaldach, M. *Prog. Biomed. Res.* **2000**, *5*, 168.
(23) Hehrlein, C. *Interventions Cardiol.* **2009**, *4*, 60−63.
(24) Yoshinobu, T.; Mitsui, H.; Tarui, Y.; Fuyuki, T.; Matsunami, H. *J. Appl. Phys.* **1992**, *72*, 2006−2013.
(25) Takahashi, K.; Nishino, S.; Saraie, J. *J. Electrochem. Soc.* **1992**, *139*, 3565−3571.
(26) Zorman, C. A.; Fleischman, A. J.; Dewa, A. S.; Mehregany, M.; Jacob, C.; Nishino, S.; Pirouz, P. *J. Appl. Phys.* **1995**, *78*, 5136−5138.
(27) Wu, C.; Jacob, C.; Ning, X.; Nishino, S.; Pirouz, P. *J. Cryst. Growth* **1996**, *158*, 480−490.
(28) Nagasawa, H.; Yagi, K. *Phys. Stat. Sol. B* **1997**, *202*, 335−358.
(29) Madapura, S.; Steckl, A. J.; Loboda, M. *J. Electrochem. Soc.* **1999**, *146*, 1197−1202.
(30) Ivanov, P. A.; Chelnokov, V. E. *Semicond. Sci. Technol.* **1992**, *7*, 863.
(31) Severino, A. *Silicon Carbide Epitaxy 3C-SiC Epitaxial Growth on Large Area Silicon: Thin Films*; Research Signpost: Kerala, India, 1992.
(32) Möller, H.; Krötz, G.; Eickhoff, M.; Nielsen, A.; Papaioannou, V.; Stoemenos, J. *J. Electrochem. Soc.* **2001**, *148*, G16−G24.
(33) Severino, A.; D'Arrigo, G.; Bongiorno, C.; Scalese, S.; la Via, F.; Foti, G. *J. Appl. Phys.* **2007**, *102*, 023518.
(34) Scholz, R.; Gösele, U.; Wischmeyer, F.; Niemann, E. *Appl. Phys. A: Mater. Sci. Process.* **1998**, *66*, 59−67.
(35) Portail, M.; Zielinski, M.; Chassagne, T.; Roy, S.; Nemoz, M. *J. Appl. Phys.* **2009**, *105*, 083505.
(36) Ollivier, M.; Latu-Romain, L.; Martin, M.; David, S.; Mantoux, A.; Bano, E.; Soulièr, V.; Ferro, G.; Baron, T. *J. Cryst. Growth* **2013**, *363*, 158−163.
(37) Li, Y.-L.; Ishigaki, T. *J. Ceram. Soc. Jpn.* **2007**, *115*, 717−723.
(38) Zhou, X.; Zhang, R.; Peng, H.; Shang, N.; Wang, N.; Bello, I.; Lee, C.; Lee, S. *Chem. Phys. Lett.* **2000**, *332*, 215−218.
(39) Beaber, A.; Girshick, S.; Gerberich, W. *Int. J. Fract.* **2011**, *171*, 177−183.
(40) Alper, J. P.; Vincent, M.; Carraro, C.; Maboudian, R. *Appl. Phys. Lett.* **2012**, *100*, 163901.
(41) Goh, B. T.; Rahman, S. A. *Mater. Chem. Phys.* **2014**, *147*, 974−981.
(42) Nazarudin, N. F. F. B.; Noor, N. J. B. M.; Rahman, S. A.; Goh, B. T. *J. Lumin.* **2015**, *157*, 149−157.
(43) Perdew, J. P.; Burke, K.; Ernzerhof, M. *Phys. Rev. Lett.* **1996**, *77*, 3865−3868.
(44) Soler, J. M.; Artacho, E.; Gale, J. D.; García, A.; Junquera, J.; Ordejón, P.; Sánchez-Portal, D. *J. Phys.: Condens. Matter* **2002**, *14*, 2745−2779.
(45) Tersoff, J. *Phys. Rev. B* **1989**, *39*, 5566−5568.
(46) Latu-Romain, L.; Ollivier, M. *J. Phys. D* **2014**, *47*, 203001.
(47) Geaney, H.; Mullane, E.; Ramasse, Q. M.; Ryan, K. M. *Nano Lett.* **2013**, *13*, 1675−1680.
(48) Amato, M.; Palummo, M.; Rurali, R.; Ossicini, S. *Chem. Rev.* **2014**, *114*, 1371−1412.
(49) Dayeh, S. A.; Tang, W.; Boioli, F.; Kavanagh, K. L.; Zheng, H.; Wang, J.; Mack, N. H.; Swadener, G.; Huang, J. Y.; Miglio, L.; Tu, K.-N.; Picraux, S. T. *Nano Lett.* **2013**, *13*, 1869.
(50) Harris, G., Ed. *Properties of Silicon Carbide*; EMIS Datareviews Series; The Institution of Engineering and Technology: London, U.K.,, 1995.
(51) Dhar, S.; Seitz, O.; Halls, M. D.; Choi, S.; Chabal, Y. J.; Feldman, L. C. J. *Am. Chem. Soc.* **2009**, *131*, 16808−16813.
(52) Vegard, L. *Z. Phys.* **1921**, *5*, 17−26.
(53) Denton, A. R.; Ashcroft, N. W. *Phys. Rev. A* **1991**, *43*, 3161−3164.
(54) Musin, R. N.; Wang, X.-Q. *Phys. Rev. B* **2005**, *71*, 155318.
(55) Iori, F.; Ossicini, S.; Rurali, R. *J. Appl. Phys.* **2014**, *116*, 154301.
(56) Amato, M.; Palummo, M.; Ossicini, S. *Phys. Status Solidi B* **2010**, *247*, 2096.
(57) Zhu, X.; Fahy, S.; Louie, S. G. *Phys. Rev. B* **1989**, *39*, 7840−7847.
(58) Goñi, A. R.; Muniz, L. R.; Reparaz, J. S.; Alonso, M. I.; Garriga, M.; Lopeandia, A. F.; Rodríguez-Viejo, J.; Arbiol, J.; Rurali, R. *Phys. Rev. B* **2014**, *89*, 045428.
(59) Ollivier, M.; Latu-Romain, L.; Salem, B.; Fradetal, L.; Brouzet, V.; Choi, J.-H.; Bano, E. *Mater. Sci. Semicond. Process.* **2015**, *29*, 218−222.

DOI: 10.1021/acs.nanolett.5b00670
Nano Lett. XXXX, XXX, XXX−XXX

(60) Choi, S.-W.; Katoch, A.; Sun, G.-J.; Kim, J.-H.; Kim, S.-H.; Kim, S. S. *ACS Appl. Mater. Interfaces* **2014**, *6*, 8281−8287.
(61) Coleman, N.; Morris, M.; Spalding, T.; Holmes, J. *J. Am. Chem. Soc.* **2001**, *123*, 187−188.
(62) Coleman, N. R. B.; O'Sullivan, N.; Ryan, K. M.; Crowley, T. A.; Morris, M. A.; Spalding, T. R.; Steytler, D. C.; Holmes, J. D. *J. Am. Chem. Soc.* **2001**, *123*, 7010−7016.
(63) Ma, D. D. D.; Lee, C. S.; Au, F. C. K.; Tong, S. Y.; Lee, S. T. *Science* **2003**, *299*, 1874−1877.
(64) Wu, Y.; Cui, Y.; Huynh, L.; Barrelet, C.; Bell, D.; Lieber, C. *Nano Lett.* **2004**, *4*, 433−436.
(65) Zhong, Z.; Fang, Y.; Lu, W.; Lieber, C. M. *Nano Lett.* **2005**, *5*, 1143−1146.
(66) De Padova, P.; Quaresima, C.; Perfetti, P.; Olivieri, B.; Leandri, C.; Aufray, B.; Vizzini, S.; Le Lay, G. *Nano Lett.* **2008**, *8*, 271−275.

DOI: 10.1021/acs.nanolett.5b00670
Nano Lett. XXXX, XXX, XXX−XXX